Monthly Notices
of the
ROYAL ASTRONOMICAL SOCIETY

MNRAS **454,** 2549–2556 (2015) doi:10.1093/mnras/stv1951

Spectral models for early time SN 2011fe observations

E. Baron,[1,2⋆] P. Hoeflich,[3] Brian Friesen,[1] M. Sullivan,[4] E. Hsiao,[5] R. S. Ellis,[6] A. Gal-Yam,[7] D. A. Howell,[8,9] P. E. Nugent,[10] I. Dominguez,[11] K. Krisciunas,[12] M. M. Phillips,[5] N. Suntzeff,[12] L. Wang[12] and R. C. Thomas[11]

[1]*Homer L. Dodge Department of Physics and Astronomy, University of Oklahoma, 440 W. Brooks, Rm 100, Norman, OK 73019-2061 USA*
[2]*Hamburger Sternwarte, Gojenbergsweg 112, D-21029 Hamburg, Germany*
[3]*Department of Physics, Florida State University, Tallahassee, FL 32306, USA*
[4]*School of Physics and Astronomy, University of Southampton, Southampton SO17 1BJ, UK*
[5]*Las Campanas Observatory, Casilla 601, La Serena, Chile*
[6]*Cahill Center for Astrophysics, California Institute of Technology, Pasadena, CA 91125, USA*
[7]*Benoziyo Center for Astrophysics, Weizmann Institute of Science, 76100 Rehovot, Israel*
[8]*Las Cumbres Observatory Global Telescope Network, Goleta, CA 93117, USA*
[9]*Department of Physics, University of California, Santa Barbara, CA 93106-9530, USA*
[10]*Computational Cosmology Center, Lawrence Berkeley National Laboratory, 1 Cyclotron Rd., Berkeley, CA 94720, USA*
[11]*Universidad de Granada C/ Bajo de Huetor 24 Aptdo 3004, E-18071, Granada, Spain*
[12]*Department of Physics and Astronomy, George P. and Cynthia Woods Mitchell Institute for Fundamental Physics and Astronomy, Texas A and M University, 4242 TAMU, College Station, TX 77843, USA*

Accepted 2015 August 20. Received 2015 August 19; in original form 2015 May 8

ABSTRACT

We use observed UV through near-IR spectra to examine whether SN 2011fe can be understood in the framework of Branch-normal Type Ia supernovae (SNe Ia) and to examine its individual peculiarities. As a benchmark, we use a delayed-detonation model with a progenitor metallicity of $Z_{\odot}/20$. We study the sensitivity of features to variations in progenitor metallicity, the outer density profile, and the distribution of radioactive nickel. The effect of metallicity variations in the progenitor have a relatively small effect on the synthetic spectra. We also find that the abundance stratification of SN 2011fe resembles closely that of a delayed-detonation model with a transition density that has been fit to other Branch-normal SNe Ia. At early times, the model photosphere is formed in material with velocities that are too high, indicating that the photosphere recedes too slowly or that SN 2011fe has a lower specific energy in the outer $\approx$0.1 $M_{\odot}$ than does the model. We discuss several explanations for the discrepancies. Finally, we examine variations in both the spectral energy distribution and in the colours due to variations in the progenitor metallicity, which suggests that colours are only weak indicators for the progenitor metallicity, in the particular explosion model that we have studied. We do find that the flux in the *U* band is significantly higher at maximum light in the solar metallicity model than in the lower metallicity model and the lower metallicity model much better matches the observed spectrum.

Key words: radiative transfer – supernovae: general – supernovae: individual: SN 2011fe.

1 INTRODUCTION

Supernova PTF11kly/2011fe (henceforth SN 2011fe) was discovered by the Palomar Transient Factory on 2011 Aug 23 in M101 only hours after explosion (Nugent et al. 2011). This nearby, early discovered object has been extremely well observed in all bands. The Carnegie Supernova Project obtained excellent spectroscopy in the infrared (Hsiao et al. 2013). Photometry has been obtained by *SWIFT* in the UV (Brown et al. 2012), in the optical (Richmond & Smith 2012; Vinkó et al. 2012; Munari et al. 2013; Pereira et al. 2013), and in the IR (Matheson et al. 2012). Pereira et al. (2013) presented a detailed comparison of the photometric observations including a well calibrated spectrophotometric time series. SN 2011fe has been observed in the radio (Chomiuk et al. 2012), in gamma-rays (Isern et al. 2013), and in the X-ray (Liu et al. 2012). From the spectra and photometry, SN 2011fe is about as ordinary an SN Ia as there could be. Due to the early discovery

⋆ E-mail: baron@ou.edu

and close proximity, several groups have drawn conclusions about the environment of SN 2011fe. Using non-detections and the very early observed points, Bloom et al. (2012) were able to constrain the radius of the primary star, concluding that it must be a compact object (white dwarf or neutron star). Using archival *HST* images, Li et al. (2011) were able to rule out luminous red giant and helium star companions. Using radio data, constraints have been placed on the progenitor environment which have been interpreted as ruling out the single degenerate scenario (Chomiuk et al. 2012); however, the winds blown during the progenitor formation could naturally produce a low-density environment that do not necessarily require a degenerate companion (see also Horesh et al. 2012).

Some spectral modelling of the optical spectra of SN 2011fe has been presented (Röpke et al. 2012; Dessart et al. 2014). Here, we want to compare and contrast SN 2011fe to a model which reproduces the spectra of a Branch-normal supernova (Sandage et al. 1996). We use a model because this allows us to translate spectral similarities and differences into physical space, for example, to determine the relevant mass layer involved in the differences. We have specifically chosen a generic delayed-detonation (DD) model for Branch-normal supernova and not tuned the model for this specific supernova. The goal of this study is to show that SN 2011fe is close to a Branch-normal supernova and to evaluate differences and discuss possible physical causes.

This study is based on the combined UV and optical *HST* and IR Gemini spectra. The infrared spectra that we study have been already were presented in Hsiao et al. (2013). The UV+optical observations were also presented and studied in previous work (Foley et al. 2012a,b; Foley & Kirshner 2013; Mazzali et al. 2014). Here, we present a detailed comparison quantitative synthetic spectroscopy with a number of epochs of SN 2011fe, all of which include coverage from the UV through the IR.

2 SPECTRAL CALCULATIONS AND EXPLOSION MODEL

We performed spectral calculations using the multipurpose stellar atmospheres program PHOENIX/1D version 16 (Hauschildt et al. 1996, 1997b; Hauschildt, Baron & Allard 1997a; Baron & Hauschildt 1998; Hauschildt & Baron 1999). Version 16 incorporates many changes over previous versions used for supernova modelling (Baron et al. 2006; Baron, Branch & Hauschildt 2007) including many more species in the equation of state (83 versus 40), twice as many atomic lines, many more species treated in full NLTE, and an improved equation of state. PHOENIX/1D solves the radiative transfer equation along characteristic rays in spherical symmetry including all special relativistic effects. The non-LTE (NLTE) rate equations for many ionization states are solved, including the effects of ionization due to non-thermal electrons from the γ-ray s produced by the radiative decay of ^{56}Ni, which is synthesized in the supernova explosion. The atoms and ions calculated in NLTE are He I–II, C I–III, O I–III, Ne I, Na I–II, Mg I–III, Si I–III, S I–III, Ca II, Ti II, Cr I–III, Mn I–III, Fe I–III, Co I–III, and Ni I–III. These are all the elements whose features make important contributions to the observed spectral features in SNe Ia.

Each model atom includes primary NLTE transitions, which are used to calculate the level populations and opacity, and weaker secondary LTE transitions which are included in the opacity and implicitly affect the rate equations via their effect on the solution to the transport equation (Hauschildt & Baron 1999). In addition to the NLTE transitions, all other LTE line opacities for atomic species not treated in NLTE are treated with the equivalent two-level atom source function, using a thermalization parameter, $\alpha = 0.10$ (Baron et al. 1996). The atmospheres are iterated to energy balance in the comoving frame; while we neglect the explicit effects of time dependence in the radiation transport equation, we do implicitly include these effects, via explicitly including $p\,\mathrm{d}V$ work and the rate of gamma-ray deposition in the generalized equation of radiative equilibrium and in the rate equations for the NLTE populations.

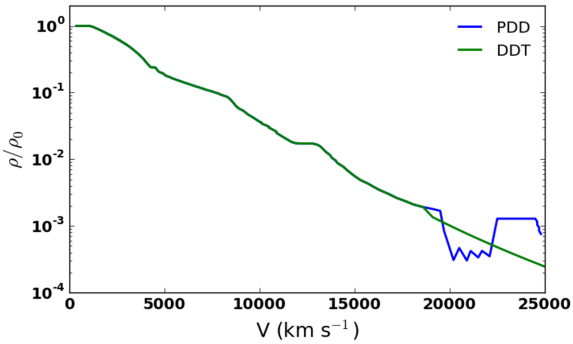

Figure 1. The density profile of the prompt DDT and the PDD that were compared. The value of ρ_0 at maximum light is about 2×10^{-12} g cm^{-3}.

The outer boundary condition is the total bolometric luminosity in the observer's frame. The inner boundary condition is that the flux at the innermost zone ($v = 700$ km s^{-1}) is given by the diffusion equation. Converged models required 256 optical depth points to correctly obtain the Si II λ6355 profile.

For our analysis, we use a DD model which reproduces the light curves and spectra for Branch-normal supernovae (Hoeflich, Khokhlov & Wheeler 1995; Hoeflich et al. 2002; Gerardy et al. 2003; Hoeflich 2006). Gerardy et al. (2003) compared a very similar model to SN 2003du for the entire range of optical to 3800 Å to 2 μm. The models start from a C/O white dwarf taken from the core of an evolved 5M$_\odot$ main-sequence star. Through accretion, this core approaches the Chandrasekhar limit. An explosion begins spontaneously when the core has a central density of 2.0×10^9 g cm^{-3} and a mass close to 1.37 M$_\odot$ (Hoeflich 2002). The transition from deflagration to detonation is triggered at a density of 2.3×10^7 g cm^{-3}. We considered two modes for the DD transition: one with a direct transition during the deflagration phase, the other after a mild pulsation which formed an envelope of 10^{-2} M$_\odot$. The resulting density structures are shown in Fig. 1. We considered initial metallicities Z of Z$_\odot$ and Z$_\odot$/20. Here, Z is defined as the iron abundance relative to solar. We take into account the smaller variation of the elements such as Ne and O compared to the Fe-group elements (Argast et al. 2001). The former dominates the metallicity effect on nuclear burning, whereas the latter sets the floor for Fe-group elements (Hoeflich, Wheeler & Thielemann 1998; Hoeflich et al. 2000).

3 RESULTS

3.1 General properties

We calculated both a classical DD model and a pulsating delayed detonation (PDD) model motivated by the report of Parrent et al. (2012) of two distinct high- and low-velocity components in the Si, O, and C lines. In Fig. 2, we show the comparison between the DD model, the PDD model, and the observations at day 2. While neither model is strongly preferred over the other, the features in the PDD model are more washed out, a trend which continues into later

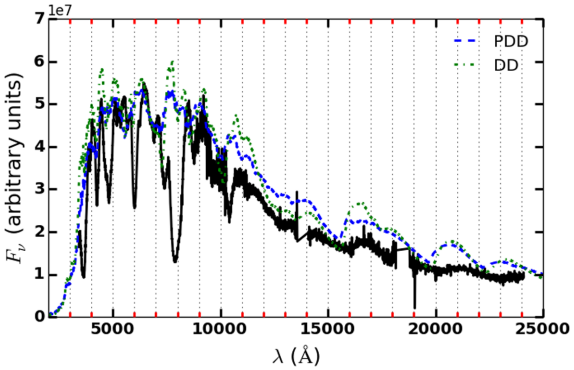

Figure 2. PDD versus DD at day 2. The spectra of the PDD model (dashed line) and the DD model (dot–dashed line) are compared to the observations (solid line).

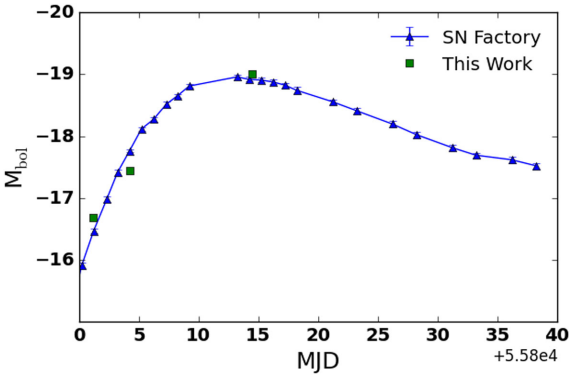

Figure 3. The bolometric light curve from these calculations compared to the bolometric light curve inferred by Pereira et al. (2013).

epochs and it indicates that the dense shell is certainly not desirable, thus we choose to use the standard DD model for this study. Our PDD model and DDT model differ somewhat from those of Dessart et al. (2014), but we find that the variation in the colours, specifically the flux in the *U* band is due to metallicity of the progenitor.

We find a preference between models with solar metallicity and $Z_\odot/20$. There are not strong differences at the earliest times, but rather at maximum light. The solar metallicity progenitor produces somewhat redder spectra in the bluest bands and we adopted a progenitor metallicity with $Z_\odot/20$ as the fiducial model. We discuss the differences in Section 4.1.

3.2 Benchmarking SN 2011fe

Having probed the primordial metallicity and explosion class, we use a DD model whose calculated light curve gives results in line with the observed class of Branch-normal supernovae as a benchmark for SN 2011fe. With time, spectra reveal increasingly deeper layers. The spectral sequence provides a key probe of the layers for similarities and differences between the model and the observations. Therefore, throughout our discussion we will identify the layers by their mass coordinate measured from the outside – more precisely, we report the location of the line forming region of the Si II λ6355 line. The velocity of both the observed and synthetic line is measured the same way, by determining the wavelength of the blueshifted minimum. Note that the UV spectra always probe the very outer layers (see fig. 11 in Hoeflich et al. 1995). Fig. 3

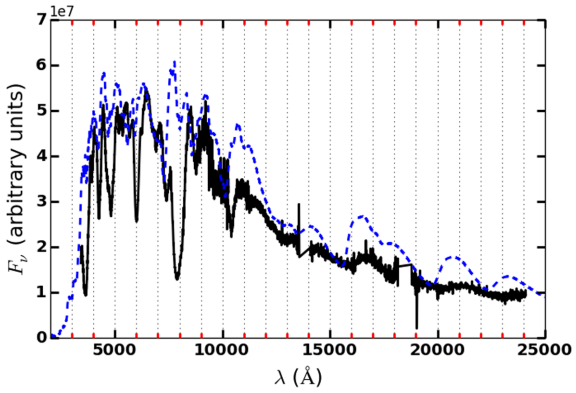

Figure 4. NLTE synthetic spectrum on day 2 (dashed line) is compared to the optical spectrum obtained at Lick on 2011 Aug 25 and the IR spectrum obtained at Gemini North on 2011 Aug 25 (solid line).

shows the bolometric light curve inferred by Pereira et al. (2013) and the values used in these calculations.

We consider epochs up to maximum light because the corresponding 'photospheric regions' undergo partial burning. Details of the spectral features are rather sensitive to small variations in brightness and non-thermal excitation (Baron et al. 2012).

Aug 25/Day 2. The earliest spectrum of SN 2011fe was obtained on Aug 25, about 2 d after the explosion, which probes the outer $5 \times 10^{-3}\,M_\odot$. The spectral features are quite sensitive to the temperature and excitation, we show the NLTE spectra in Fig. 4. We calculated an LTE model with the same parameters and the LTE model is much too bright in the IR and the features are weak, compared to the NLTE model. The figures show that almost all the lines present in the observed spectrum are also in the synthetic spectrum. While many of the line strengths are well reproduced by the model, the Si II λ6355 line is much too weak and the Si II λ5970 line is about the right strength, but is too fast. The LTE model overpredicts the IR flux and the IR features are weak, whereas the NLTE model roughly gets the IR continuum correct, but the IR features are too strong and broad. A common feature of both the LTE and NLTE spectra is a too large Doppler shift of all the absorption features of intermediate-mass elements both in the optical and IR, including the Ca II IR-triplet and the O I λ7773.4 line. As mentioned above, details of the line features are very sensitive to excitation and temperature effects. In particular, a higher Doppler shift may be produced by an excessive emission component seen for example in Mg II λ10926 or O I λ7773.4. However, even in case of LTE, the trend is confirmed. The smaller Doppler shifts in SN 2011fe compared to the DD model for a Branch-normal supernova may be attributed to a lower specific energy or photosphere that recedes more quickly.

Aug 28/Day 5. Fig. 5 shows the comparison to the combined *HST*+optical+IR spectrum obtained on MJD 55801.12 which probes the outer $3 \times 10^{-2}\,M_\odot$. The overall spectral shape from UV through optical is quite well reproduced. The far-UV is a bit high, but the quality of the fit from 0.2−2.5 μm is quite good. the Si II λ6355 line is about the right strength, the Si II λ5970 line is too strong and fast by about 4000 km s^{-1}, as is the Ca IR triplet. Actually, the the Si II λ5970 line is low by about 20 per cent, but it does not recover to the blue as the observed spectrum does, due to blending with other lines. In general, the spectrum is somewhat too fast.

Aug 31/Day 8. Fig. 6 shows the comparison to the combined *HST*+optical+IR spectrum obtained on MJD 55804.25 which probes the outer $5 \times 10^{-2}\,M_\odot$. Not only is the overall spectral

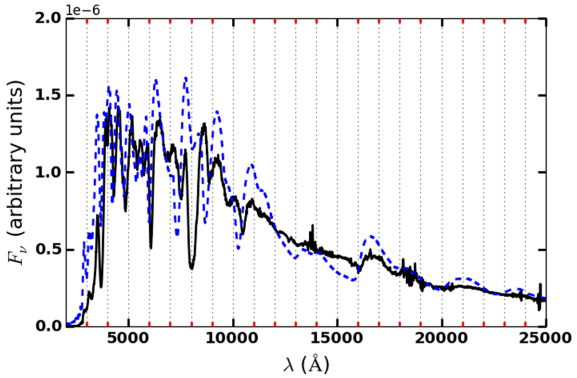

Figure 5. NLTE synthetic spectrum on day 5 (dashed line) is compared to the UV/optical spectrum obtained by *HST* on on 2011 Aug 28 (MJD 55801.12) and the IR spectrum obtained at Gemini North on 2011 Aug 28 (solid line).

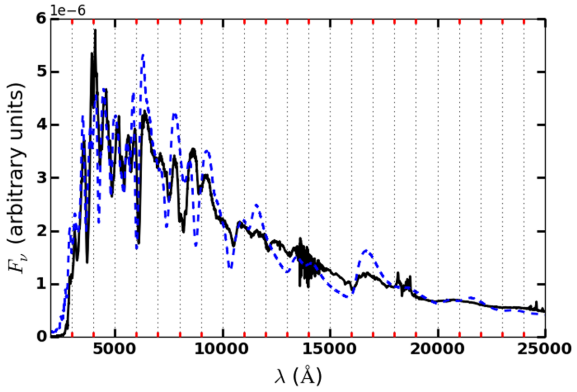

Figure 6. NLTE synthetic spectrum on day 8 (dashed line) is compared to the UV/optical spectrum obtained by *HST* on on 2011 Aug 31 (MJD 55804.25) and the IR spectrum obtained at Gemini North on 2011 Aug 31 (solid line).

shape from UV through optical quite well reproduced, but also the relative strength of the far-UV closely matches the observations. However, the iron and silicon feature around 4000 Å is too weak. The strength of Ca II H+K is well reproduced. The calcium IR triplet is now too narrow, and not strong enough in absorption. The Si II λ6355 line is well fit in absorption strength, but it is too fast by about 4000 km s^{-1} and the emission peak is about 20 per cent too high, indicating that the model at this phase is too extended. The Si II λ5970 line is now also well fit in absorption. The Mg II λ9226 line is much too strong. The Mg II λ10926 feature is too strong as are most of the rest of the features further to the red in the IR. The O I λ7773.4 line is prominent, but too strong and too broad. The Si II λ11714.87 feature is prominent in the synthetic spectrum, but much weaker in the observed spectrum.

Sep 10/Day 18. In Fig. 7, we show the spectrum obtained on MJD 55814.43 which which is close to maximum light (Nugent et al. 2011; Pereira et al. 2013) which probes the outer 0.5 $M_\odot$. For reference, Pereira et al. (2013) find $t_{B_{\max}}$ on MJD 55814.51. The observed spectrum of SN 2011fe closely resembles the synthetic spectrum for a Branch-normal supernova both with respect to the line strength and the Doppler shifts of individual lines. Overall the Doppler shifts are consistent, but the model is slightly too cool, resulting in a reduced flux in the blue. This could be due to either strong line blanketing in the blue, which pushes flux to the red or because the opacities due to the iron group elements decrease in the blue as the temperature decreases. The complex formation of the observed spectrum was studied in Bongard et al. (2008). The Si II λ6355 line is now in good agreement in both absorption and emission strength, indicating that the model at this phase has about the correct velocity extension. The Si II λ5970 line now is also well fit in both absorption and emission (modulo the too low pseudo-continuum). The Ca II IR triplet is too weak. The Mg II λ9226 and Mg II λ10926 features are too strong, as are most of the rest of the features further to the red in the IR.

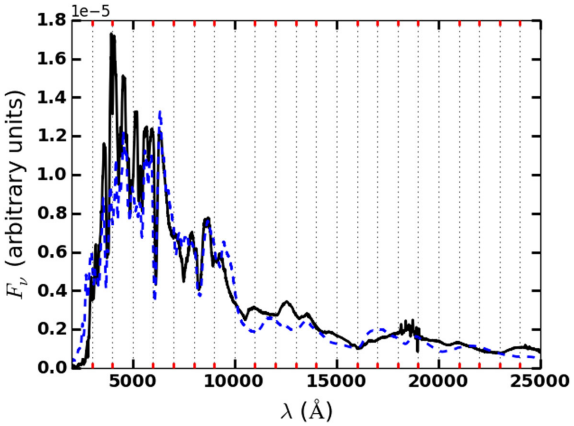

Figure 7. NLTE synthetic spectrum on day 18 (dashed line) is compared to the UV/optical spectrum obtained by *HST* on on 2011 Sep 10 (MJD 55814.43) and the IR spectrum obtained at Gemini North on 2011 Sep 10 (solid line).

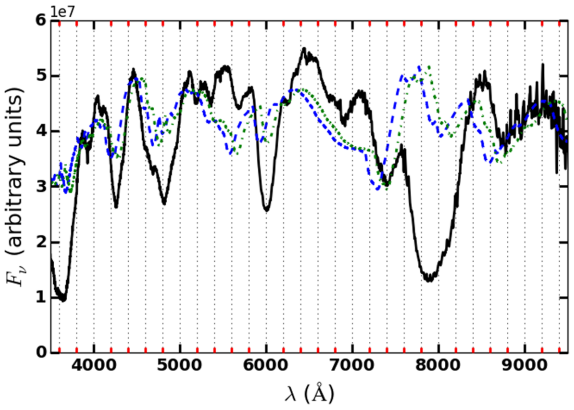

Figure 8. Optical blow up of Aug 25 spectrum (solid line) shown in Fig. 4 where the synthetic spectra are shown with (dot–dashed line) and without (dashed line) a 'redshift' of $z = 0.015$.

4 DISCUSSIONS AND CONCLUSION

Fig. 8 shows the optical spectra of the Aug 25 spectrum we have modelled, along with the synthetic spectra shifted by a 'redshift' $z = 0.015$. Similar experiments give 'redshift' values of 0.015, 0.015, 0.010, for Aug 28, Aug 31, and Sep 10, respectively. This shows that the recession of the pseudo photosphere in the hydro model with time is slower than in the observations. We can estimate the amount of the shift by comparing the velocity of the absorption minimum of Si II λ6355 line at each epoch. Table 1 shows the measured minimum velocity for each epoch. Since the velocity is close at maximum light we will consider the 'outer part' of the model to be at velocities $v \geq 11\,300$ km s^{-1}.

Table 1. Velocities of the absorption minimum of Si II λ6355 feature at each epoch in km s^{-1}.

Si II λ6355 velocities		
Epoch (Day) (since explosion)	$V_{\rm Si\,II}$ (observed)	$V_{\rm Si\,II}$ (synthetic)
2	16 300	20 700
5	13 000	17 300
8	11 300	16 000
18	9 700	10100

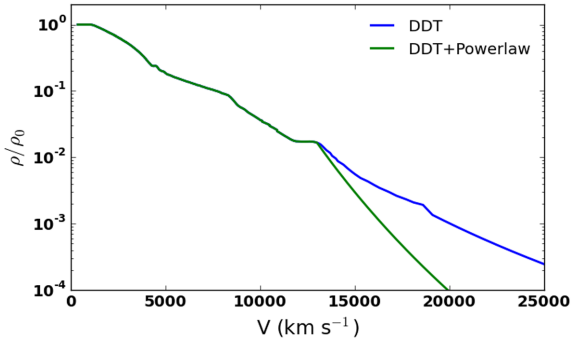

Figure 9. The original density profile of the hydro model is compared to a modified profile where the density is forced to follow a power law $\rho \propto (v/v_{\rm cut})^{-n}$, for velocities $v > v_{\rm cut}$, where $v_{\rm cut} = 12\,000$ km s^{-1}, and $n = 12$.

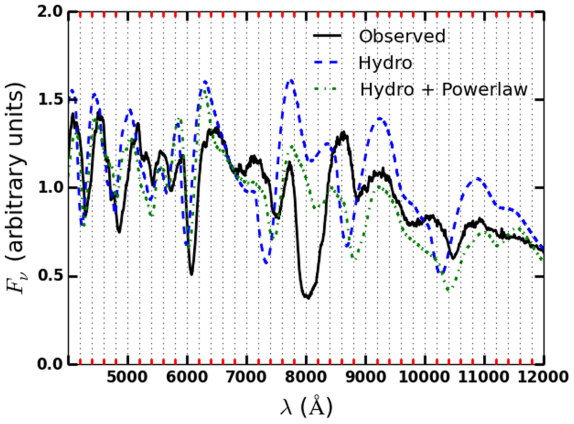

Figure 10. NLTE spectra day 5 original hydro model (dashed line) compared to model hydro model with density profile $\rho \propto v^{-12}$ for $v > 12\,000$ km s^{-1} (dot–dashed line). The observed spectrum is shown with a solid line.

We can reduce the effective velocity extension by steepening the density profile beyond the photosphere. This can be produced by an outwardly increasing specific energy with mass element. While steeper density profiles violate energy conservation from nuclear burning and make the models hydrodynamically inconsistent, we perform an empirical exercise to examine its effect on the synthetic spectra, being careful not to generalize the results too much. Fig. 9 shows the modified density profile, obtained by forcing the density to follow a power law $\rho \propto (v/v_{\rm cut})^{-n}$, for velocities $v > v_{\rm cut}$, where we took $v_{\rm cut} = 12\,000$ km s^{-1}, and $n = 12$ (Branch et al. 2005, 2007, 2006, 2008; Branch, Dang & Baron 2009; Doull & Baron 2011). Fig. 10 shows a comparison of the Aug 28/Day 5 spectrum with and without the density profile modification. The effects of the density modification are largest in the red and smaller in the blue. The Si II λ6355 is somewhat slower and the line profile is clearly narrower, but the agreement is not significantly better. However, in the red, the shape of the O I λ7773.4 line is much better and that continues on to the Ca II IR triplet, the Mg II λ9226 feature, and the Mg II λ10926 feature. In the modified density structure the Si II λ11714.87 becomes more pronounced. Thus, while steepening the density profile does not significantly improve the agreement, it does have some benefit in moving the absorptions of the redder lines to the correct velocity.

A full study of the possible reasons for lower observed photospheric velocities is beyond the scope of the current study. Some possible reasons for lower velocities can be understood within the framework of spherical DD models. For a wide range of model parameters the overall density structures are very similar (Hoeflich, Müller & Khokhlov 1993). A possible reason for the lower observed photospheric velocity may be a faster receding photosphere in mass. To first order for 1–2 weeks past maximum light in Branch-normal SNe Ia, the opacities remain high and the photosphere recedes in mass due to geometrical dilution of the expanding envelope (Hoeflich et al. 1993). In order to increase the recession rate of the pseudo-photosphere, we need a lower kinetic energy. In classical DD models, most of the matter undergoes burning. Possible ways to reduce the kinetic energy include higher binding energy of the white dwarf and thus, higher central densities; less nuclear energy production due to a smaller C/O ratio, by, for example, a larger main-sequence mass; less heating in the outer layers by ^{56}Ni by shifting its distribution to the central layers. We are not signalling out one particular cause and to do so is beyond the scope of this work. We note that Baron et al. (2012) suggested that a higher value of C/O could explain the high velocities seen in SN 2001ay, whereas Ohlmann et al. (2014) found that varying the C/O ratio alone in a fixed white dwarf did not have dramatic effects.

PDD models with a large amount of unburned material will reduce the explosion energy proportional to the amount of unburned material, and may lower the velocities of elements of incomplete burning. However, strong pulsations produce an outer, high velocity layer as observed in, for example, SN 1990N and similar SNe Ia (Quimby et al. 2006). An alternative explanation is significantly lower mass progenitor than the Chandrasekhar mass which, would be less luminous and inconsistent with the light curve.

4.1 Progenitor metallicity

Fig. 11 compares the synthetic spectra of the fiducial progenitor model with $Z = Z_\odot/20$ to that of progenitor with solar metallicity. The other explosion parameters were the same for both models. By eye, prior to maximum light, there is not a clear preference for either model, which is somewhat surprising since naïvely one expects progenitor metallicity to play a role at particularly early times. At maximum light a strong discrepancy appears, where the solar metallicity progenitor appears too blue or more accurately, the flux is much higher in the *U* band. To attempt to quantify this, we calculated synthetic photometry on both the observations and the models and compared the colours. This procedure is subject to systematic errors since it assumes that the relative flux of the observations is very accurate, so that the synthetic colours calculated from the observed spectra are meaningful. Given this caveat, we did not find a clear preference for either progenitor metallicity, based *solely* on colours. We examined the 25 filters from *HST* and the Johnson set *UBVRIJHK*$_s$ and looked at all combinations of neighbouring blue filter - red filter. The lack of clear trends can be seen in the bluest filters *F*220*W*–*F*250*W*, the models are too red at

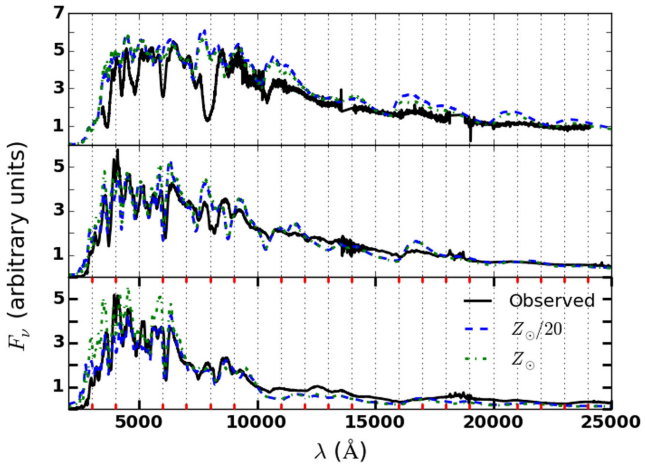

Figure 11. The synthetic spectra of the $Z = Z_\odot/20$ (dashed line) and the $Z = Z_\odot/20$ (dot–dashed line) progenitor model compared to observations (solid line) for days Aug 25 (top panel), Aug 31 (middle panel), and Sep 10 (bottom panel).

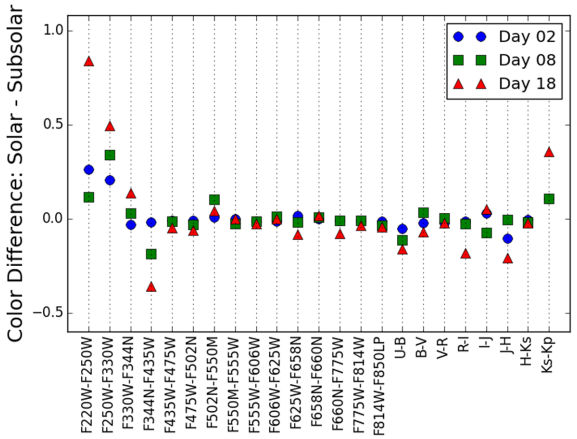

Figure 12. The difference in 23 synthetic colours for $Z = Z_\odot$ the $Z = Z_\odot/20$ progenitor model compared for days Aug 25, Aug 31, and Sep 10. The colours are plotted from bluest to reddest filters and the difference plotted is, for example, $(B-V)_{Z_\odot} - (B-V)_{Z_\odot/20}$. The filters used are in order from blue to red, *HST*/ACS-HRC: *F220W*, *F250W*, *F330W*, *F344N*, *F435W*, *F475W*, *F502N*, *F550M*, *F555W*, *F606W*, *F625W*, *F658N*, *F660N*, *F775W*, *F814W*, *F850LP*, *F892N*; UBVRI+2MASS: *U,B,V,R,I,J,H,K*. We did not calculate colours across the filter sets, so the *F892N-U* colour is not plotted.

day 2, and too blue at days 8 and 18, in the *F250W–F330W* filters, the models are significantly too blue at day 2, but then only slightly too blue at days 8 and 18. The discrepancy is far smaller in the *F330W–F344N* and *F344N–F435W* colours, with the same trend and then changes in the *F435W–F475* colour where the models are too blue at day 2, too red at day 8 and then the solar model is slightly too blue and the sub-solar model slightly too red at day 18. Fig. 12 shows the differences in the 23 different colours at the three different epochs studied. The trend for the solar metallicity model to become much redder in the bluest bands at maximum light is evident, but it is difficult to discern an overall pattern in the colours. In the bluest filters, the solar metallicity model is much redder at maximum light, until we reach the *F435W–F475W* colour, where the solar metallicity model suddenly becomes bluer than the lower metallicity model, redwards there is no strong trend in the colours.

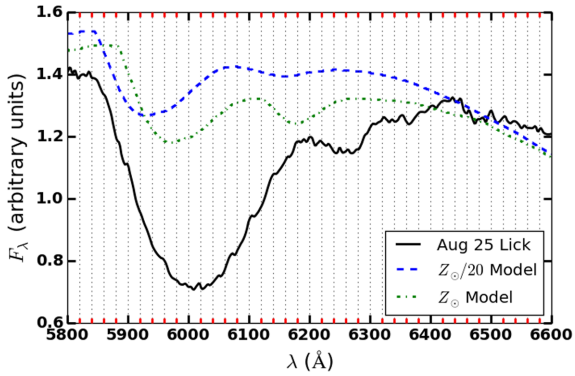

Figure 13. The synthetic spectra of the $Z = Z_\odot$ (dashed line) and the $Z = Z_\odot/20$ (dot–dashed line) progenitor model compared to the observation (solid line) on Aug 25. While both models show a line due to C II λ6580, the solar metallicity model line is about the right shape and strength as the observed feature. However the velocity minima are at 15 000 km s^{-1} in the observations, 18 000 km s^{-1} in the solar metallicity model and 19 000 km s^{-1} in the model with $Z = Z_\odot/20$.

Prior to maximum light, there is really no strong trend in the colours at any wavelength. The largest discrepancy is in fact evident from Fig. 11 where the solar metallicity model is clearly much brighter in the *U* band. In fact, the solar metallicity model is nearly 0.5 mag brighter than the low metallicity model in *U*, even though both models are blue in $U - B$ and the solar metallicity model is only about 0.1 mag bluer in $U - B$ than the low metallicity model. Thus, one really needs spectra in the rest-frame *U* band to try to get a handle on progenitor metallicity.

Overall, the results make sense, in the bluest colours, particularly at maximum light, the solar metallicity model is much redder than the lower metallicity model due to higher opacities in the UV, but clear diagnostics are not so evident. Our results are in good agreement with those of Hoeflich and collaborators (Hoeflich et al. 1998; Hoeflich et al. 2000). Mazzali et al. (2014) found evidence for a progenitor metallicity of $Z_\odot/2$, which is not inconsistent with our results.

Fig. 13 shows that the C II λ6580 appears with roughly the strength and shape as does the observed feature in the solar metallicity model at on Aug 25, while not at the correct Doppler shift. The velocities of the feature are (15 000, 18 000, 19 000) km s^{-1} for the observations, the solar metallicity progenitor, and the low metallicity progenitor, respectively. We have confirmed the identification of the line as due to C II in the models by rerunning the spectra with the C II line opacity set to zero. This gives credence to claims of C II in other SNe Ia (see Thomas et al. 2007, 2011; Parrent et al. 2011; Parrent 2015; Folatelli et al. 2012, and references therein).

Weaker C II and higher Si velocities can be understood in terms of the variation in the progenitor evolution. At the end of the central He-burning and therefore, in mixtures which are helium poor, $^{12}C(\alpha, \gamma)^{16}O$ results in lower C/O ratios in the convective core. With lower metallicity, the size of the convective core decreases due to lower opacities. Shell burning will produce material with $C/O \approx 1$. As a result of less carbon, the explosion energy for our progenitors decreases with *Z*. With higher explosion energy, we expand faster and for a given DDT, the very outer layers are burned at higher density reducing the amount of material in the unburned layers and resulting in a higher expansion velocities (Hoeflich et al. 1998; Hoeflich et al. 2000, 2010).

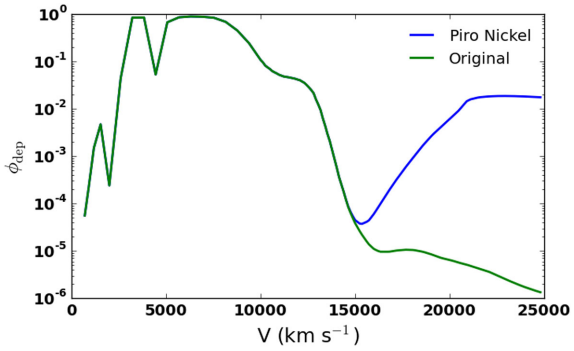

Figure 14. The deposition function at day 2, using the model nickel distribution and the one obtained by using the prescription of Piro (2012).

4.2 Enhanced Nickel mixing?

We examine a suggestion of Piro (2012) who by studying the early rise of the light curve concluded that ^{56}Ni was required in the outer $0.1 < M < 1 \times 10^{-3}$ of the supernova. He further concluded that this requirement places constraints on the explosion model, somewhat favouring models where the detonation begins in the outer parts of the star. Piro's 2012 study is based on the diffusion time-scales for the rise time. In fact, geometrical dilution will be responsible for the receding of the photosphere and adiabatic expansion of the corresponding layers must be taken into account. Fig. 14 shows the γ-ray deposition function (the γ-ray deposition function is the ratio of the rate of absorption of γ-rays κJ to the instantaneous decay rate of ^{56}Ni, see, for example, Sutherland & Wheeler 1984; Jeffery 1998) for our standard case, compared to that obtained using the prescription of Piro (2012). We chose to make the mass fraction of radioactive nickel constant at $X_{^{56}\mathrm{Ni}} = 0.03$ above a velocity of 15 500 km s^{-1}, which corresponds to a mass of 0.1 M$_\odot$ masses from the outer boundary. This is about in the middle of the parameter choices outlined in Piro (2012). In our model the bottom layer where the ^{56}Ni is added occurs at a velocity of $v \sim 15\,500$ km s^{-1}. Thus, the photosphere in our model is significantly above this modified heating region. Nevertheless, we find negligible changes due to the added heating. The temperature of our models is a little higher in the outer parts, but not enough higher in the low-density environment to significantly alter the observed spectra. Fig. 14 explains this result: the γ-ray deposition function ϕ_{dep} is increased by the extra nickel only up to the level of $\sim 1 \times 10^{-3}$, but only at the highest velocities and not near the photosphere. The increase in deposition is not enough to dramatically change the outer energy deposition rate at day 2.

4.3 Comparison to other work

Light curves and spectra of SN 2011fe at these epochs have been studied by Röpke et al. (2012), Foley (2012), Foley & Kirshner (2013), Dessart et al. (2014), Mazzali et al. (2014), and Graham et al. (2015). Röpke et al. (2012) compared the fidelity of a DD Chandrasekhar mass model and violent merger model to the observations of the Nearby Supernova Factory and found that both models had their shortcomings, but found no strong preference for either model. Mazzali et al. (2014) performed abundance tomography on a *W7* model and a DD model and found that the DD model was somewhat preferable, in addition to finding a primordial metallicity that was about half solar. Dessart et al. (2014) studied PDD models in general, and found a preference for a PDD model to match the B-band light curve of SNe 2011fe and the spectral evolution. However, their PDD models have much weaker shells then the model we considered (compare their fig. 10 to Fig. 1). They also find very washed out features at early epochs (see their fig. 16). Foley & Kirshner (2013) used empirical comparisons with the models of Lentz et al. (2000) to find a low metallicity for SN 2011fe of about Z$_\odot$/4 and a ratio between the metalicity of SN 2011by and SN 2011fe of about 30. Graham et al. (2015) found the that UV flux in the assumed supersolar SN 2011by is significantly lower than that in SN 2011fe, in rough agreement with the *W7*-based models of Lentz et al. (2000), but in contradistinction to the DD models used in this work. Thus, overall our results are generally compatible with those of previous work.

5 CONCLUSIONS

We have compared *HST* and ground based spectra of SN 2011fe up to maximum light to detailed NLTE synthetic spectra of a Branch-normal hydrodynamic model. Progenitor models with metallicities of of Z$_\odot$ and Z$_\odot$/20 qualitatively show overall reasonable results after day 2 based on optical spectra.

We explored the possibility that the high-velocity feature reported by Parrent et al. (2012) may be produced by a shell as a result of a 'low-amplitude pulsation'. Though a shell may produce a high-velocity feature, it also would produce high fluxes in the UV and U wavelengths inconsistent with the observations as well as the very high velocity photosphere at early times, which leads to washed out features (Section 3 and Dessart et al. 2014). Branch normal models show features at the corresponding wavelengths produced by iron-group elements (Gerardy et al. 2003).

Nearly all the features in the observed spectra are seen in the synthetic spectra in approximately the correct range of the velocity, that is, the elemental stratification in the model also appears in the observations. However, as discussed in Section 3.2, the photosphere in the model is formed at too high velocities at early times corresponding to the outermost 0.05–0.1 M$_\odot$. In principle, this can be corrected by a smaller kinetic energy of the explosion, e.g. by higher central densities and, thus, higher binding energy, or high C/O ratios in the progenitor. Alternatively, the photosphere of SN 2011fe may recede faster due to lower excitation of ions (from gamma-rays or the radiation field) and/or variations in the density structure. In SN 2011fe, the second explanation is favoured because, by maximum light, the photospheric velocities of the model and SN 2011fe are in close agreement (see Table 1).

There are a multiple ways that the adopted model could be adjusted to reproduce the observed discrepancies, including variations in the chemical structure, rotation of the progenitor, or pulsations prior and during the explosion (although this would have to done in accord with constraints from observed spectra). Future studies will examine these effects in detail.

ACKNOWLEDGEMENTS

We thank Aaron Dotter for help in constructing the synthetic photometry with a wide choice of filters. We also thank the anonymous referee for improving the presentation of this work. The work has been supported in part by support for programmes HST-GO-12298.05-A, and HST-GO-12948.04-A was provided by NASA through a grant from the Space Telescope Science Institute, which is operated by the Association of Universities for Research in Astronomy, Incorporated, under NASA contract NAS5-26555. This work was also supported in part by the NSF, AST-0709181, AST-0707704, AST-0708855, AST-0708873. This research was also

supported, in part, by the NSF grant AST-0703902 to PAH. The work of EB was also supported in part by SFB 676, GRK 1354 from the DFG. ID has been supported in part by the Spanish Ministry of Science and Innovation project AYA2008-04211-C02-02 (ID). This research used resources of the National Energy Research Scientific Computing Center (NERSC), which is supported by the Office of Science of the US Department of Energy under Contract No. DE-AC02-05CH11231; and the Höchstleistungs Rechenzentrum Nord (HLRN). We thank both these institutions for a generous allocation of computer time.

REFERENCES

Argast D., Samland M., Gerhard O. E., Thielemann F.-K., 2001, Ap&SS Suppl., 277, 193
Baron E., Hauschildt P. H., 1998, ApJ, 495, 370
Baron E., Hauschildt P. H., Nugent P., Branch D., 1996, MNRAS, 283, 297
Baron E., Bongard S., Branch D., Hauschildt P., 2006, ApJ, 645, 480
Baron E., Branch D., Hauschildt P. H., 2007, ApJ, 662, 1148
Baron E., Hoeflich P., Krisciunas K., Dominguez I., Khokhlov A. M., Phillips M. M., Suntzeff N., Wang L., 2012, ApJ, 753, 105
Bloom J. S. et al., 2012, ApJ, 744, L17
Bongard S., Baron E., Smadja G., Branch D., Hauschildt P., 2008, ApJ, 687, 456
Branch D., Baron E., Hall N., Melakayil M., Parrent J., 2005, PASP, 117, 545
Branch D. et al., 2006, PASP, 118, 560
Branch D. et al., 2007, PASP, 119, 709
Branch D. et al., 2008, PASP, 120, 135
Branch D., Dang L. C., Baron E., 2009, PASP, 121, 238
Brown P. J. et al., 2012, ApJ, 753, 22
Chomiuk L. et al., 2012, ApJ, 750, 164
Dessart L., Blondin S., Hillier D. J., Khokhlov A., 2014, MNRAS, 441, 532
Doull B., Baron E., 2011, PASP, 123, 765
Folatelli G. et al., 2012, ApJ, 745, 74
Foley R. J., 2012, ApJ, 748, 127
Foley R. J., Kirshner R. P., 2013, ApJ, 769, L1
Foley R. J. et al., 2012a, AJ, 143, 113
Foley R. J. et al., 2012b, ApJ, 752, 101
Gerardy C. et al., 2003, ApJ, 607, 391
Graham M. L. et al., 2015, MNRAS, 446, 2073
Hauschildt P. H., Baron E., 1999, J. Comp. Appl. Math., 109, 41
Hauschildt P. H., Baron E., Starrfield S., Allard F., 1996, ApJ, 462, 386
Hauschildt P. H., Baron E., Allard F., 1997a, ApJ, 483, 390
Hauschildt P. H., Schwarz G., Baron E., Starrfield S., Shore S., Allard F., 1997b, ApJ, 490, 803
Hoeflich P., 2002, New Astron. Rev., 46, 475
Hoeflich P., 2006, Nucl. Phys. A, 777, 579
Hoeflich P., Müller E., Khokhlov A., 1993, A&A, 268, 570
Hoeflich P., Khokhlov A., Wheeler J. C., 1995, ApJ, 444, 831
Hoeflich P., Wheeler J. C., Thielemann F.-K., 1998, ApJ, 495, 617
Hoeflich P., Nomoto K., Umeda H., Wheeler J. C., 2000, ApJ, 528, 590
Hoeflich P., Gerardy C., Fesen R., Sakai S., 2002, ApJ, 568, 791
Hoeflich P. et al., 2010, ApJ, 710, 444
Horesh A. et al., 2012, ApJ, 746, 21
Hsiao E. et al., 2013, ApJ, 766, 72
Isern J. et al., 2013, A&A, 552, A97
Jeffery D. J., 1998, preprint (astro-ph/9811356)
Lentz E., Baron E., Branch D., Hauschildt P. H., Nugent P., 2000, ApJ, 530, 966
Li W. et al., 2011, Nature, 480, 348
Liu J., Di Stefano R., Wang T., Moe M., 2012, ApJ, 749, 141
Matheson T. et al., 2012, ApJ, 754, 19
Mazzali P. A. et al., 2014, MNRAS, 439, 1959
Munari U., Henden A., Belligoli R., Castellani F., Cherini G., Righetti G. L., Vagnozzi A., 2013, New Astron., 20, 30
Nugent P. E. et al., 2011, Nature, 480, 344
Ohlmann S. T., Kromer M., Fink M., Pakmor R., Seitenzahl I. R., Sim S. A., Röpke F. K., 2014, A&A, 572, A57
Parrent J. T., 2015, MNRAS, preprint (astro-ph/1412.7163)
Parrent J. T. et al., 2011, ApJ, 732, 30
Parrent J. T. et al., 2012, ApJ, 752, L26
Pereira R. et al., 2013, A&A, 554, A27
Piro A. L., 2012, ApJ, 759, 83
Quimby R., Hoeflich P., Kannappan S., Rykoff E., Rujopakarn W., Akerlof C., Gerardy C., Wheeler J. C., 2006, ApJ, 636, 400
Richmond M. W., Smith H. A., 2012, J. Am. Assoc. Var. Star Obs., 40, 872
Röpke F. K. et al., 2012, ApJ, 750, L19
Sandage A., Saha A., Tammann G., Labhardt L., Panagia N., Macchetto F. D., 1996, ApJ, 460, L15
Sutherland P., Wheeler J. C., 1984, ApJ, 280, 282
Thomas R. C. et al., 2007, ApJ, 654, L53
Thomas R. C. et al., 2011, ApJ, 743, 27
Vinkó J. et al., 2012, A&A, 546, A12

This paper has been typeset from a TEX/LATEX file prepared by the author.